ELSEVIER

Materials Science and Engineering A292 (2000) 162–168

MATERIALS SCIENCE & ENGINEERING A

www.elsevier.com/locate/msea

Phase change phenomena during high power laser-materials interaction

Xianfan Xu *, Kevin H. Song

School of Mechanical Engineering, Purdue University, West Lafayette, IN 47907-1288, USA

Abstract

This work investigates phase change phenomena due to high power pulsed laser irradiation. During high power laser heating, the intense radiation flux from the laser is transformed to the target material and raises the temperature of the target surface rapidly. When the laser fluence is high enough, melting and superheating of liquid are possible. At even higher laser fluences, the superheated liquid undergoes a phase explosion that turns the liquid into a mixture of liquid and vapor. In this paper, we describe theoretical, numerical and experimental studies of the materials' response under nanosecond pulsed excimer laser irradiation. Experiments are performed in a laser fluence range between 2.5 and 10 J/cm^2 (between 100 and 400 MW/cm^2) on nickel specimens. The velocity of the laser-evaporated vapor, absorption of the laser energy by the laser-evaporated vapor, the threshold laser fluence for phase explosion, and the pressure and temperature at the target surface are determined. Results of these studies reveal phase change mechanisms during high power laser interaction with metal.

Keywords: Phase change phenomena; High power; Laser-materials interaction

1. Introduction

High power excimer lasers are being used in a variety of applications, including micro machining and pulsed laser deposition of thin films. During these processes, the laser beam evaporates and ionizes the target material, creating a plasma plume above the target surface. Understanding the energy transport process between the laser and the target, the materials removal mechanisms, and the transport process of the laser beam in the laser-induced plasma plume is essential for controlling the laser-materials interaction and optimizing the processes.

The most important parameters needed to be understood in the laser ablation process are the transient surface temperature and the transient surface pressure. The surface temperature determines the degrees of superheating in the liquid. When the liquid is superheated to a thermodynamic stability limit, explosive type of phase change occurs. On the other hand, the surface pressure determines the evaporation rate. When it is high enough, the surface pressure causes 'flushing' of the liquid out of the melt pool. This work investigates the materials removal mechanisms based on some of our recent experimental studies. The velocity of the laser-evaporated plume is measured, and is used to estimate the surface temperature and pressure using gas dynamic relations. Optical properties of the laser-evaporated plume are also measured, which are needed in the gas dynamic calculation to account for the energy addition in the laser-evaporated plume. The pressure due to evaporation is measured using a PVDF transducer. These time-resolved measurements are performed in the laser fluence range from 2.5 to 10.5 J/cm^2 (between 100 and 400 MW/cm^2) on nickel specimens. Using the measured data, together with the gas dynamics modeling of the laser ablated plume, the transient temperature and pressure at the target surface during laser ablation are obtained.

In what follows, evaporation mechanisms during laser-metal interaction are introduced first. Details of experiments for measuring the vapor velocity, vapor optical properties, and the evaporation pressure are then described, and the results are presented. A simplified gas dynamic model is used to estimate the surface temperature at different laser fluences. Results of these studies will determine phase change mechanisms

* Corresponding author.
E-mail address: xxu@ecn.purdue.edu (X. Xu).

0921-5093/00/$ - see front matter
PII: S0921-5093(00)00996-5

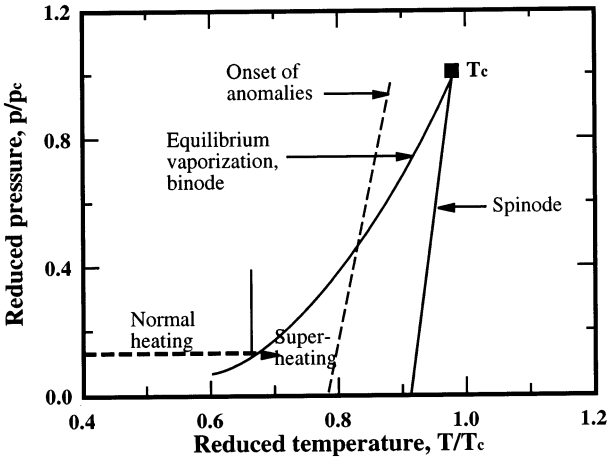

Fig. 1. p-T diagram.

during high power, pulsed excimer laser interaction with metal.

2. Evaporation mechanisms

Under high power pulsed laser irradiation, the surface of the target can be melted and evaporated, and the temperature of the liquid can be raised above the boiling point. To illustrate the heating process by a pulsed laser, the p-T diagram is shown in Fig. 1 [7]. The 'normal heating' line indicates the heating process of liquid metal when the temperature is below the boiling temperature. At the boiling temperature, the liquid and vapor phases are in equilibrium, which is shown in Fig. 1 as the intersection between the normal heating line and the binode line. The binode line is the equilibrium phase change relation between surface temperature and vapor pressure calculated from the Clausius-Clapeyron equation. When the surface temperature of a liquid is below or at the boiling temperature, evaporation occurs at the liquid surface, which is a type of heterogeneous evaporation.

Under rapid heating, it is possible to heat the liquid metal to temperatures above the boiling point. The superheating process is represented by the 'superheating' line in Fig. 1. In a slow heating process, the surface temperature-pressure relation follows the Clausius-Clapeyron relation, i.e. the heating path follows the binode. However, when the heating rate is fast enough, the heating process could deviate from the binode, and follow a superheating line shown in Fig. 1. In this case, the liquid is superheated.

The existence of the superheated state depends on the rate of spontaneous nucleation during heating. The rate of spontaneous nucleation can be determined from the Döring and Volmer's theory [5]. Using this theory, it has been shown that the frequency of spontaneous nucleation is about 0.1 s^{-1} cm^{-3} at the temperature near 0.89 T_c, where T_c is the thermodynamic critical temperature, but increases to 10^{21} s^{-1} cm^{-3} at 0.91 T_c [4]. This indicates a rapidly heated liquid could possess considerable stability with respect to spontaneous nucleation up to 0.89 T_c, with an avalanche-like onset of spontaneous nucleation of the entire high temperature liquid layer at about 0.91 T_c. At a temperature of about 0.91 T_c, homogeneous nucleation, or explosive phase transformation occurs, which turns the entire superheated liquid to a mixture and vapor leaving the surface like an explosion.

The above description defines an upper limit for superheating, which is shown as the spinode in Fig. 1. The spinode temperature can also be obtained from the thermodynamic considerations when the material loses thermodynamic phase stability as calculated by the second derivatives of the Gibbs' thermodynamic potential [4]. As the temperature approaches the spinode, the fluctuations ΔV and ΔH increase sharply, with $(\partial p/\partial V)_T \rightarrow 0$ and $(\partial T/\partial S)_p \rightarrow 0$. A loss of thermodynamic stability occurs, leading to phase explosion of the superheated liquid.

During pulsed excimer laser heating, radiation energy from the laser beam is transformed to thermal energy within the radiation penetration depth, which is about 10 nm for Ni at the KrF excimer laser wavelength (248 nm). Superheating is possible since the excimer laser pulse is short, on the order of 10^{-8} s. Within this time duration, the amount of nuclei generated by spontaneous nucleation is small at temperatures below 0.9 T_c, thus the liquid can be heated to the metastable state. Depending on the laser fluence, the target surface can be melted, and the liquid can successively undergo the normal heating process, the superheating process and the explosive phase change. Heterogeneous evaporation occurs at the liquid surface when the laser fluence is low. However, when the laser intensity is high enough to induce explosive phase transformation, physical phenomena associated with laser ablation are dominated by explosive vaporization.

The theory described above was developed over two decades ago during the study of the pulsed current heating of metal. The intent of this work is to provide experimental evidences of different phase change mechanisms during pulsed laser heating. This information is critical for understanding of the materials removal process induced by a pulsed laser and applications involving a pulsed laser.

3. Experimental studies

The laser used in this work is a KrF excimer laser ($\lambda = 248$ nm) with a 30 ns pulse width (FWHM). The center, uniform portion of the excimer laser beam

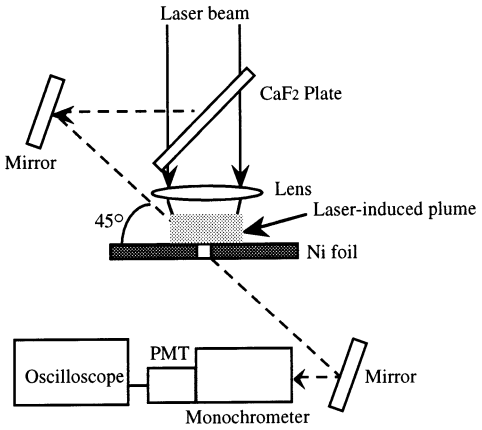

Fig. 2. Setup for the measurement of transient transmissivity of the laser-induce vapor plume.

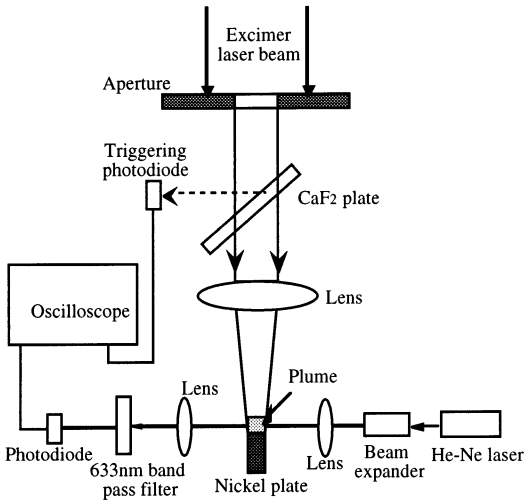

Fig. 3. Experimental setup for measuring the velocity of the shock front and the vapor front.

passes through a rectangular aperture (10 by 5 mm) to produce a laser beam with a uniform intensity profile. The rectangular laser beam is focused onto the nickel specimen and evaporates the target surface. The laser-evaporated surface was examined under an optical microscope. It was found that the center 90% of the laser-irradiated area was uniform. A single 150-mm focal length CaF_2 lens is used to focus the laser beam on the target. The spot size is varied by translating the lens along the optical axis. The laser fluence (energy density per pulse) is varied through changing the spot size at the target surface and attenuation of energy per pulse. Energy per laser pulse at the target surface is calibrated using an energy meter. The energy variation is monitored through a built-in energy meter of the excimer laser. A fast silicon photodiode sensing a split beam from the excimer laser beam is used to trigger the data acquisition system.

3.1. Measurement of optical properties of the laser ablated plume

Optical properties of the laser-ablated plume will provide information regarding to absorption of the laser beam by the plume. The thickness of this plume can be as thin as a few micrometers during the initial stage of its formation, and grows to about 100 μm at the end of the laser pulse. To detect optical properties of such a thin layer, a special experimental set-up is designed. Fig. 2 shows the experimental set-up for this measurement. Details of this measurement were described elsewhere [9]. A probing beam is split from the excimer laser beam by a CaF_2 plate and is directed to the center of the specimen by a dielectric mirror. The specimen is a 5 μm-thick, freestanding nickel foil. To measure the transmissivity of a thin plasma layer, a circular pinhole with a diameter, d of 10–12 μm is fabricated at the center of the specimen. The transmission of the probing beam through the pinhole is measured. If the plasma layer is thicker than $\delta tan(\theta) - d$, the entire probing laser beam passes through the plasma layer, and the path length of the probing beam in the plasma can be determined using straight-forward geometry calculations. Here d, δ and θ denote the thickness of the nickel film, the diameter of the pinhole, and the angle of the probing beam measured from the normal direction of the specimen, respectively. For a 5 μm-thick film with a pinhole diameter of 10 μm, and at the probing beam angle of 45°, transmission of the plasma layer with a minimum thickness of 5 μm ($\delta\ tan(\theta) - d$) can be measured.

A photo-multiplier tube (PMT) is used to capture the transmitted light through the monochromator and record the transient intensity of the probing beam on an oscilloscope. Comparison between the intensity of the probing beam with and without the plume yields the transient transmissivity of the plume.

3.2. Measurement of the velocity of the laser ablated plume

The velocity of the laser-ablated plume is related to the surface temperature and pressure, and therefore will provide information on the ablation mechanism. Fig. 3 shows the experimental set-up for measuring the velocity of the laser-induced plasma using the optical deflection technique. The probing laser for the optical deflection measurement is a 5 mW, He-Ne laser with a wavelength at 633 nm. The He-Ne laser beam is focused to a 10 μm spot above the Ni target surface, and its intensity is measured by a photodiode. The width of the nickel specimen is about 100 μm, shorter than the depth of focus of the probing beam. A narrow band pass filter at the He-Ne laser wavelength is positioned in front of the detecting photodiode to eliminate

plasma emission. The laser-induced shock wave and the vapor front deflect the HeNe laser beam, which is sensed by the photodiode and recorded on the oscilloscope. The oscilloscope, triggered by the laser pulse, measures the time elapse between the beginning of laser pulse and the fluctuations of the probing beam.

The distance between the probing He-Ne laser beam and the specimen surface is adjusted by an x-y micrometer-stage from near zero to 500 μm. At different distances, the arrival times of the shock front and the vapor front are recorded. The measured distance-time relations are the transient locations of the shock front and the vapor front. The velocities of the shock wave and the vapor front are calculated from the transient locations of the shock front and the vapor front.

3.3. Measurement of the laser induced shock wave in the target

When the laser fluence is above the ablation threshold, the recoil pressure due to the ablated material leaving the target surface produces a shock wave propagating into the target. Time resolved stress profile induced by laser beam heating in the nickel target is measured using a polyvinylidene fluoride (PVDF) piezoelectric transducer [8]. The PVDF transducer is a newly developed stress sensor. It presents several advantages including high time resolution (~ 1 ns), large measurement range (0.1 bar to 10 Mbar), and large signal output. In addition, the PVDF transducer is highly reproducible under recurrent shock loading, which is often lacked in conventional piezoelectric film shock sensors. Under shock loading, the PVDF transducer delivers a voltage $V(t)$ proportional to the stress difference between the two surfaces of the PVDF transducer foil [1]:

$$V(t) = [\sigma_f(t) - \sigma_b(t)]/l \quad (1)$$

where $\sigma_f(t)$ and $\sigma_b(t)$ are, respectively, the shock history at the front and the back face of the transducer. Fig. 4 shows the detailed assembly of the target and PVDF transducer. The target is a 242 μm-thick nickel foil (99.95% purity). Before taking data at a laser fluence, the target surface is pre-treated using multiple laser pulses at that laser fluence. Thin adhesive resin (Teflon, Polytetrafluoroethylene), of which shock impedance is matched to PVDF, holds the target to the PVDF transducer. A 25.5 mm-thick Kel-F (polychlorotrifluoroethylene) buffer, whose shock impedance is also matched to PVDF, is used to mount the PVDF transducer and is fitted into an aluminum canister. The canister is 1 inch in diameter and 2 inches long. The PVDF transducer is connected via a BNC cable to an oscilloscope, which is set to the 50 Ω terminal load resistance for fast data acquisition.

The excimer laser fluence is varied from 0.7 to 6 J/cm^2. Higher fluences are not obtained in this experiment, since the laser spot size has to be kept larger than the size of the PVDF transducer, which is about 1×1 mm. The stress profile in the nickel target is obtained from the measured stress profile in the PVDF transducer using the shock impedance mismatch method with the known Hugoniot equations of state of nickel and the PVDF material [8].

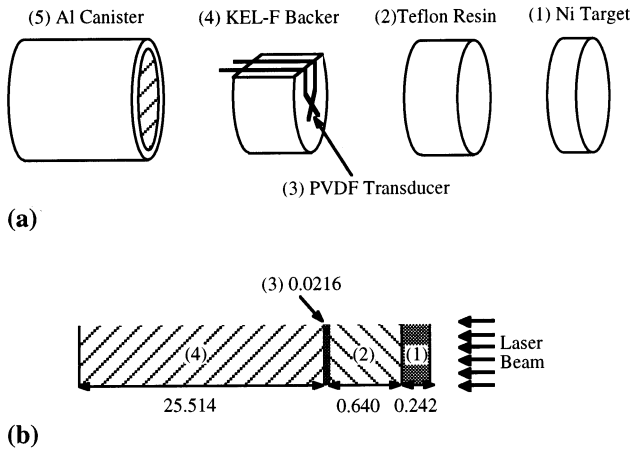

Fig. 4. Detailed target and PVDF transducer assembly.

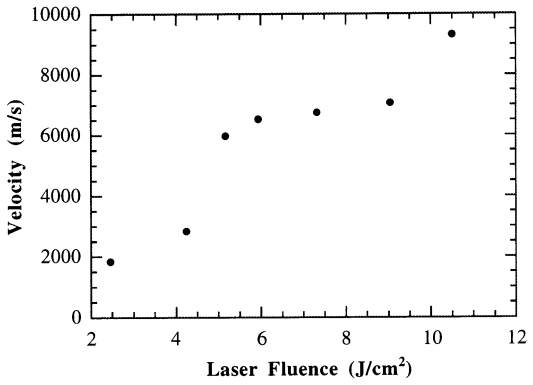

Fig. 5. Velocity of the laser-evaporated plume.

3.4. Experimental results

Fig. 5 shows the velocity of the laser-evaporated plume as a function of the laser fluence. These are averaged velocity values within the laser pulse width. The experiment showed that the velocity of the plume front decayed slightly ($\sim 10\%$) within the laser pulse width. The time-averaged velocity increases with the laser fluence increase, from ~ 2000 m/s at the lowest fluence to ~ 9000 m/s at the highest fluence. However, the increase of velocity is not monotonous; the velocity increases slightly when the laser fluence is low. A sudden jump of the velocity is seen at the laser fluence of about 4.2 J/cm^2. Between 5.2 and 9 J/cm^2, the velocity is almost a constant.

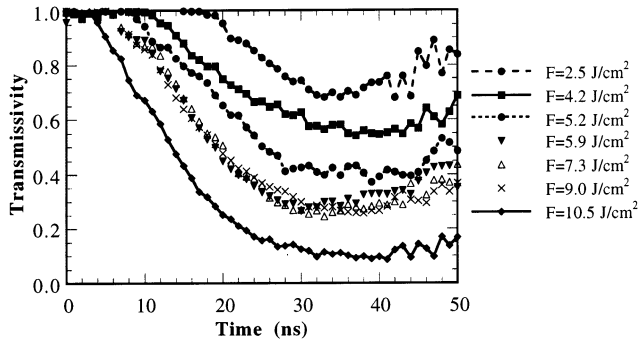

Fig. 6. Transient transmissivity of the laser-evaporated plume.

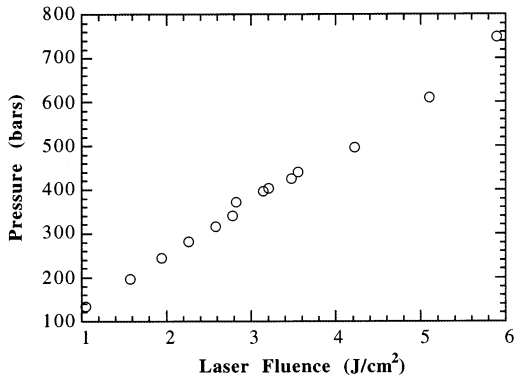

Fig. 7. Peak pressure in the nickel target.

The variation of the velocity increase with the laser fluence indicates that different laser ablation mechanisms occur in the laser fluence range used in the experiment. The velocity of the plume is determined by the pressure and the temperature at the target surface. The constant velocity in the medium fluence region indicates that the surface temperature is not affected by the increase of the laser fluence in the medium fluence region. Such a constant surface temperature can be explained as a result of explosive evaporation. As discussed earlier, the maximum surface temperature during explosive phase transformation is about 0.9 T_c, the spinodal temperature. Once the laser fluence is high enough to raise the surface temperature to the spinode, further increase of the laser fluence would not raise the surface temperature. On the other hand, in the low fluence region, the velocity increases over 50%. Therefore, the surface temperature increases with the laser fluence increase; heterogeneous vaporization occurs at the surface. At the highest laser fluence, the velocity of the plume is higher than that of the middle region. This could be due to a higher absorption rate of the laser energy by the plume, as shown in the transmission measurement (Fig. 6). Absorption of laser energy by the plume further raises the temperature of the plume and increases the plume velocity.

Fig. 6 shows the transient transmissivity of the plume at different laser fluences. The transmissivity remains at '1' for the first several nanoseconds, which corresponds to the period before generation of the plume. Transmissivity starts to decrease at an earlier time at higher laser fluences since evaporation occurs earlier at higher fluences. It can be seen that the plume generation time obtained in this experiment matches with that measured by the optical deflection technique during the velocity measurement. For certain laser intensity, the transmissivity of the plume decreases with time. The variation of transmissivity with laser intensity also shows three regions: transmissivity is almost identical for the laser fluences between 5.2 and 9 J/cm^2. This laser fluence range corresponds to the same range in which the velocity of the plume changes little with the laser fluence, i.e. extinction of the laser beam in the plume does not vary with the laser intensity in the medium fluence region.

The transmission data also indicate that the explosive phase change occurs at laser fluences above 5.2 J/cm^2. Extinction of the laser beam is determined by the cross section of the energized atoms, which in turn is determined by the temperature of the plume. The temperatures of the evaporant in the medium fluence range are all about the same since the temperatures at the surface are all about 0.9 T_c. Thus, transmission of the plume stays at a constant value. At the highest laser fluence, transmissivity decreases from that of the middle fluence range, indicating the increase of absorption of laser light by the plume.

All the experimental results consistently show that laser ablation is due to heterogeneous evaporation when the laser fluence is below 5.2 J/cm^2, and explosive phase change dominates the evaporation process when the laser fluence is higher than the 5.2 J/cm^2 threshold value. Measurements of scattering intensity of the laser beam by the laser ablated plume and heat transfer modeling also indicate a transition from normal surface evaporation to the explosive phase change at a laser fluence around 5.2 J/cm^2 [10].

Measured peak pressures in the target due to laser evaporation are shown in Fig. 7. The peak pressure increases almost linearly with increasing laser fluence, with a variation between 17 bar to 760 bar when the laser fluence varies from 1 to 6 J/cm^2.

4. Gas dynamics analysis of the laser-induced plume

The flow of the laser-evaporated vapor is described according to the model developed by Knight [2]. When the laser fluence is higher than the ablation threshold but less than the threshold for explosive phase change, the flow process is depicted in Fig. 8a. The laser-evaporated vapor leaves the target surface with a half

Maxwellian distribution. Collisions among vapor establish thermodynamic equilibrium in a layer called the Knudsen layer. From the exit of the Knudsen layer, the vapor experiences an expansion, compressing the air ahead of the vapor at the contact front. The compressed air propagates into the ambient air, forming a shock wave.

When the laser fluence is higher than the threshold for explosive phase change, the superheated liquid turns into a mixture of liquid and vapor propagating into the air as shown in Fig. 8b. The exact detail in the liquid/vapor mixture is complicate, and is not discussed in this work. The mixture also forms a contact front with the air, and the compressed air propagates into the ambient, forming a shock.

4.1. Gas dynamics model for surface evaporation

Based on the model described above, it is possible to relate the measured velocity of the shock wave and the absorption coefficient of the plume to the temperature and pressure at the surface. Therefore, the measured data described before can be used to estimate the surface conditions. Procedures of relating the measured vapor velocity to the surface parameters are described as follows.

The velocity of the shock wave is related to the pressure and temperature behind the shock, p_{ca}, T_{ca}, by the Hugoniot equation [3] as:

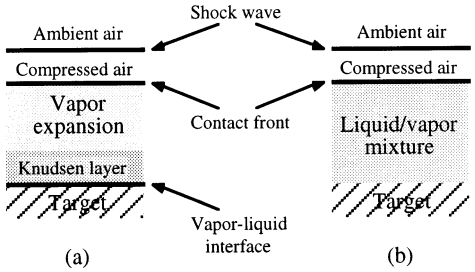

Fig. 8. One-dimensional gas dynamic models: (a) surface evaporation (b) explosive phase change.

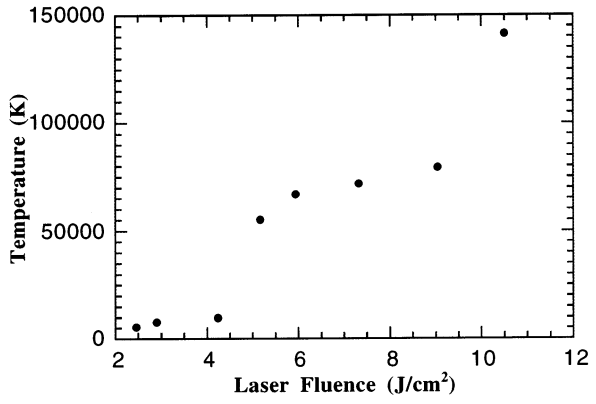

Fig. 9. Surface temperature calculated by the gas dynamics model.

$$\frac{p_{ca}}{p_{amb}} = 2\left[\frac{\gamma_{air}}{\gamma_{air}+1}\right]\cdot M_{sh}^2 - \left[\frac{\gamma_{air}-1}{\gamma_{air}+1}\right] \quad (2a)$$

$$\frac{T_{ca}}{T_{amb}} = \frac{(2\cdot\gamma_{air}\cdot M_{sh}^2-(\gamma_{air}-1))\cdot((\gamma_{air}-1)\cdot M_{sh}^2+2)}{((\gamma_{air}+1)\cdot M_{aa})^2} \quad (2b)$$

The velocity of the shock is embedded in the Mach number of the shock, $M_{sh}\cdot\gamma_{air}=1.4$ is the ratio of specific heats of air.

It is assumed that the pressure, temperature and the velocity are uniform in the compressed air, therefore, at the contact front, the pressure, temperature, and the velocity of Ni vapor, p_{cf}, T_{cf}, and v_{cf}, are the same as those of the compressed air. The relations between the temperature and pressure at the contact front and at the exit of the Knudsen layer, T_{KL} and p_{KL}, are:

$$c_p\cdot T_{cf}+0.5v_{cf}^2+P_{abs}=c_p\cdot T_{KL}+0.5v_{KL}^2 \quad (3a)$$

$$p_{cf}+\rho_{cf}\cdot v_{cf}^2=p_{KL}+\rho_{KL}\cdot v_{KL}^2 \quad (3b)$$

where c_p is the specific heat of nickel vapor, P_{abs} is the absorbed laser power by the plume, and ρ is the density. The conservation equations of mass, momentum and energy are used to establish the relationship between the thermodynamic properties at the target surface and at the exit of the Knudsen layer. For the laser fluence used in this work, it has been shown that the Mach number at the exit of the Knudsen layer is one [6]. In this case, the following relations apply:

$$T_{KL}=0.669T_{sur} \quad (4a)$$

$$p_{KL}=0.375p_{evap} \quad (4b)$$

Using Eqs. (2)–(4), along with the measured shock velocity and the absorption coefficient of the laser power by the plume, the temperature at the target surface, T_{sur}, and the evaporation recoil pressure, p_{evap}, can be estimated.

4.2. Results of the gas dynamics calculation

The calculated surface temperature is shown in Fig. 9. Note that, although the temperature is calculated for the entire laser fluence range used, the computational method is only applicable to surface evaporation; computations of the surface temperature during phase explosion are not attempted. It is seen that the surface temperature at the laser fluence of 2.5 J/cm^2 is about 5700 K, above the normal boiling point but lower than the critical temperature of nickel, 7810 K. At the laser fluence of 2.9 J/cm^2, the surface temperature reaches 7766 K. At the laser fluence of 4.2 J/cm^2, the surface temperature is about 9600 K, exceeding the critical value. However, it should be noted that the above computations carry a large uncertainty due to various assumptions and simplifications used in the calculation, including steady-state flow, constant materials proper-

ties, and neglecting dissociation of air. Therefore, from these calculations, it is not likely to determine the surface temperature accurately. On the other hand, when the laser fluence is above 5 J/cm^2, the calculated temperature is more than five times higher than the critical temperature, which would not come from inaccuracies in the computational model. Since the liquid surface can not process such a high temperature, it is concluded again, from the gas dynamics calculations that phase explosive must have occurred at laser fluences higher than 5 J/cm^2.

Calculations show that, at the laser fluence of 2.5 J/cm^2 the calculated pressure is 300 bars, which is close to the measured value (Fig. 7). The calculated evaporation pressures are 700 and 818 bars at 2.9 and 4.2 J/cm^2, while the measured values are about 380 and 500 bars, respectively. Again, exact matching between the measured and the calculated pressures are not expected, due to the assumptions and simplifications used in the calculation.

5. Conclusions

Pulsed laser ablation at different laser fluences was studied experimentally. Time-resolved measurements were performed to determine the velocity of the laser-induced plume, transmission (absorption) of the laser beam in the plume, and the evaporation recoil pressure in the laser fluence range between 2.5 and 10.5 J/cm^2. The measured velocity and absorptivity of the plume were used in a gas dynamics calculation to estimate the surface temperature and pressure. Results of different experiments and calculations consistently showed that, surface evaporation occurred when the laser fluence was below 4 J/cm^2. When the laser fluence was higher than 5 J/cm^2, evaporation was an explosive type phase change.

Acknowledgements

Support by the National Science Foundation under grant number CTS-9624890 is gratefully acknowledged.

References

[1] M. Boustie, S. Couturier, J.P. Romain, D. Zagouri, H. Simonnet, Laser Particle Beams 14 (2) (1996) 171–179.
[2] C.J. Knight, AIAA J. 17 (1979) 519–523.
[3] H.W. Liepmann, Roshko, A., Wiley, New York, 1973.
[4] M.M. Martynyuk, Russian J. Phys. Chem. 57 (1983) 494–501.
[5] V.P. Skripov, Wiley, New York, 1974.
[6] K.H. Song, X. Xu, Appl. Phys. A 65 (1997) 477–485.
[7] K.H. Song, X. Xu, Appl. Surface Sci. 127–129 (1998a) 111–116.
[8] K.H. Song, X. Xu, Proc. 1998 ASME Int. Mech. Eng. Congress Exposition, HTD-Vol. 361-4 (1998b) 79–86.
[9] X. Xu, K.H. Song, J. Heat Transfer 119 (1997) 502–508.
[10] X. Xu, G. Chen, K.H. Song, Inter. J. Heat Mass Transfer 42 (1999) 1371–1382.